

High-Performance Nanogel-in-Oils as Emulsion Evolution Controller for Displacement Enhancement in Porous Media

Xukang Lu and Moran Wang*



Cite This: *ACS Appl. Mater. Interfaces* 2023, 15, 49554–49566



Read Online

ACCESS |



Metrics & More



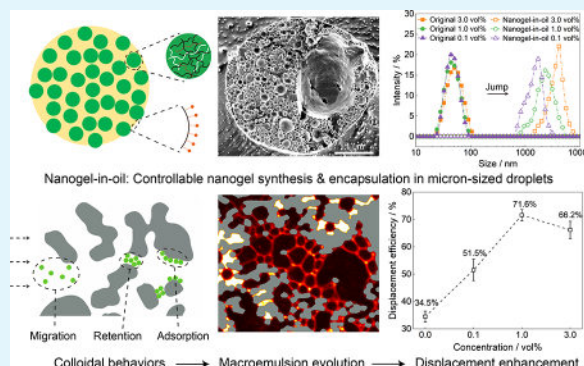
Article Recommendations



Supporting Information

ABSTRACT: We designed and synthesized high-performance nanogel-in-oils with intermediate properties between solid particles and liquid droplets for multiphase flow control in porous media. The ultrasmall polymeric nanogels prepared via inverse emulsion polymerization were efficiently encapsulated in micrometer-sized oil droplets with the aid of surfactants during transfer from the oil phase to the aqueous phase. The composite colloidal system exhibited high loading capacity, unimodal size distribution, and long-term kinetic stability in suspension. The colloidal behaviors of nanogel-in-oils and the corresponding interfacial evolution during displacement in porous media were investigated via microfluidic experiments. In situ emulsification was observed with a state contrary to that of static characterizations. The spontaneous and sustainable formation of foam-like water-in-oil macroemulsions originated from aqueous phase breakup and oil film development, both enhanced by nanogel-in-oils. Sweeping efficiency enhancement by invasion events and residual oil transport in macroemulsion phases yielded exceptional displacement performances. Flow field fluctuations and emulsion state variations can be manipulated by adjusting nanogel-in-oil concentrations. The nanogel-in-oil suspension was found to exhibit optimal performance among the tested dispersed systems.

KEYWORDS: polymeric nanogel, particle encapsulation, colloidal state, macroemulsion, multiphase displacement, porous media



1. INTRODUCTION

Dispersed systems, such as particle suspensions and emulsions, have been broadly employed for multiphase flow control in porous media. Examples include but are not limited to hydrocarbon recovery,^{1,2} remediation of contaminated soil and groundwater,^{3,4} carbon dioxide utilization,⁵ and delivery systems in human bodies for pharmaceuticals and nutraceuticals.^{6,7} Flow control can be achieved not only by adjusting interfacial parameters and fluid properties but also by inducing flow field fluctuations and phase state variations. The complex interfacial evolution process may lead to significantly higher displacement performances.

Polymeric gel particles, with sizes ranging from millimeters to nanometers, are regarded as promising agents due to their stability, tunability, and deformability.^{8–11} Microgel particles at the millimeter and micrometer scale have been developed as effective additives to block high-permeability zones and divert the invading fluid into low-permeability layers.^{12,13} The plugging effect can be achieved by single-particle blockage or multi-particle bridging depending on particle sizes.^{14–17} The size-matching rule has been extensively discussed in previous studies, whereas the optimal ratio between the particle diameter and the characteristic pore size remained controversial.^{8,18–20} In recent years, nanogel particles at the nanometer scale have drawn great

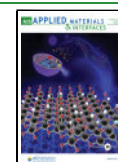
attention owing to their better injectivity and potential interfacial effects. Many studies focused on the trade-off between injectivity and plugging efficiency.^{21–23} The advances in synthesis methodology provided nanogels with intriguing properties, such as delayed swelling behaviors and enhanced mechanical strength. The adsorption of nanogel particles at the solid surface and liquid–liquid interface and their impact on fluid properties have also been investigated.^{24–26} However, the important role of adjusting the suspension composition and colloidal state in manipulating particle behaviors seemed to be overlooked.

In food and biomedical disciplines, fabrication of composite gel particle systems has already been proposed for various applications, such as emulsion gel particles for biolubrication and microgel-in-liposomes mimicking corneocyte cell structures.^{27–30} For multiphase flow control in porous media, the synthesis of micro/nanogel particles commonly involves inverse

Received: April 18, 2023

Accepted: September 25, 2023

Published: October 16, 2023



polymerization in the oil phase for the precise control of the particle size.^{31,32} The formed gel particles are usually precipitated, dried into powders, and then redispersed in water. Another approach is to directly dilute the stock suspension in the aqueous phase and release the particles via demulsification. A recent work by Lei et al. discovered microgel-in-oils by increasing the oil content in suspension.³³ Most microgel particles were released, while some were trapped in oil and formed aggregates with a cluster size of hundreds of micrometers. Microgel-in-oils were found to moderately plug the high-permeability pathways and be broken as plain microgel particles accumulate. For nanogel particles, the ultrasmall size is expected to induce different colloidal states and thereby different multiphase flow patterns. As the particle size decreases, the release process might be naturally suppressed, and the suspension state can be completely altered with the aid of stabilization agents.

Emulsions, either macro- or microemulsions, are also strong candidates for displacement enhancement.^{34,35} Surfactants are most widely adopted for emulsification, which settle on the liquid–liquid interfaces and reduce the interfacial tension (IFT) to a great extent. The addition of particles can further stabilize the emulsion structure and increase the apparent viscosity.³⁶ Similar to gel particles, injection of oil-in-water macroemulsions has been found to inhibit preferential flow and enhance sweeping efficiency.^{37–39} The preparation of these macroemulsions requires intense energy input and shear actions. In situ emulsification during the injection of surfactant or alkaline solutions has also been visualized by microfluidic experiments.^{40–42} Microemulsion phases can be spontaneously generated at the interface under such conditions, whereas sufficient phase mixing is hard to achieve during low-speed flow in porous media.

In the present study, inspired by previous efforts on composite colloidal system fabrication, we designed and synthesized nanogel-in-oils via encapsulating polymeric nanogel particles in oil droplets with a controllable and repeatable procedure. Microscopic characterizations confirmed the composite state of nanogel-in-oils as the dominant component of the suspension. Visualization and quantification of displacement processes in complex porous media by microfluidic experiments revealed remarkable displacement enhancement effects with a non-monotonic trend versus concentration. In situ development of macroemulsions can be induced and manipulated by nanogel-in-oils. Comparative experiments using other dispersed systems were further performed to elucidate the high performance of the nanogel-in-oil suspensions. Our results provide new insights into the design and application of composite nanogel systems with a more pronounced impact on interfacial evolution and less restriction on material selection.

2. EXPERIMENTAL SECTION

2.1. Nanogel-in-Oil Fabrication and Suspension Preparation.

All chemicals were purchased from Macklin Biochemical Co., Ltd. (Shanghai, China) without further purification. The original nanogel particles with a targeted size of 50 nm were synthesized via the inverse emulsion polymerization method. For a typical synthesis process, acrylamide (24.0 wt %) was first dissolved in deionized water (20.0 wt %). The anionic monomer (4.0 wt %, sodium acrylate), third monomer (2.0 wt %, *N*-vinylpyrrolidone), and a cross-linking agent (0.3 wt %, *N,N'*-methylenebis(acrylamide)) were added sequentially and stirred until clear. The pH value was adjusted to approximately 7.0 using sodium hydroxide (NaOH). Surfactants (24.0 wt %, Span 80 and Tween 60) were dissolved in solvent 1 (25.0 wt %, mineral oil), and the

monomer solution was added gradually into the oil phase while stirring continuously. The photoinitiator (0.2 wt %, azobis(isobutyronitrile)) was then dissolved in solvent 2 (0.5 wt %, toluene) and added into the above system. The mass fractions denoted in the brackets refer to the proportion of the corresponding component to the total mass of the reaction system. Finally, the photopolymerization and cross-linking reactions were conducted applying UV radiation for 15–30 min under deoxygenation condition after purging with nitrogen gas. The reactor temperature was controlled at 5–10 °C for the stabilization of the system and control of the particle size. The nanogel particles were fluorescently labeled for visualization via introducing fluorescein into the reaction system. The fluorescence would remain inside nanogels and not enter the surrounding oil phase.

After completing the polymerization process, additional hydrophilic surfactant (5 wt %, Tween 60) was added for dispersion in the aqueous phase. The stock suspension composed of nanogels, oil, and surfactants was diluted to desired volume fractions (0.1–3.0 vol %) in deionized (DI) water, which was mixed by gentle shaking and then stirred at 600 rpm for 30 min. After standing for 2–4 h, the excess oil in the upper layer was removed, and the uniform aqueous suspension was taken as the sample for characterization and displacement experiments. We also diluted the stock suspension in mineral oil to the same concentrations as that for particle size characterizations, where the nanogels remained in the original state.

Several other injection fluids were prepared for comparison. First, microgel particle suspensions with similar size as nanogel-in-oils were synthesized via inverse suspension polymerization.^{18,43} The microgel particles were completely released into the aqueous phase after mixing. Second, by the removal of monomers from the synthesis system described above, the stock solution without nanogels can be obtained, which was then diluted in the aqueous phase to prepare oil-in-water emulsions. Third, by precipitation and washing in ethanol, nanogels in the stock suspension can be extracted and then dried into powders. Purified nanogel particle suspensions, excluding oil and surfactants, were prepared by redispersing nanogel powders in DI water.

We measured the dry weight of the extracted nanogel powders to evaluate the polymer content in the prepared stock suspension, which was found to be 26.9 ± 2.3 wt %. The measured polymer content was slightly lower than the expected one due to mass loss during the precipitation and washing process. Information on the chemical composition of nanogels was obtained by Fourier transform infrared (FTIR) spectroscopy analysis with a Nicolet iS50 spectrometer (Thermo Fisher Scientific, USA).

2.2. Suspension Characterization. A droplet of the prepared nanogel-in-oil suspension was placed onto a glass slide and covered with a coverslip. The suspension state and particle distribution were observed via an inverted fluorescence microscope (Nikon Ti2, Japan). The in situ microscopic morphology of nanogel-in-oils in the suspension was characterized using a cryoscanning electron microscope (Cryo-SEM, Helios NanoLab G3UC, USA), equipped with a Quorum PP3010T cryo-system.

The particle size distribution and zeta potential were measured by a Zetasizer Nano-ZS system (Malvern Instruments, UK) based on dynamic light scattering (DLS). Rheology tests were performed using a rotational rheometer (Haake Mars III, Thermo Fisher Scientific, USA) equipped with a cone–plate geometry (C60/1° TiL) at ambient temperature.

2.3. Interfacial Parameter Measurements. Interfacial parameters were characterized using a drop shape analyzer (DSA 25, Krüss, Germany). Contact angle measurements were conducted by placing an aqueous droplet onto the silicon substrate submerged in a decane-filled reservoir. Before each experiment, all substrates were ultrasonically cleaned with acetone, absolute ethanol, and DI water for 10 min sequentially and then dried and immersed in the oil-filled reservoir. The aqueous contact angle was determined using the Young–Laplace fitting method, and the time evolution was recorded. The above measurements are used to characterize intrinsic wettability conditions. Interfacial tension (IFT) measurements were performed for aqueous fluid/decane systems by using the pendant drop method. To capture

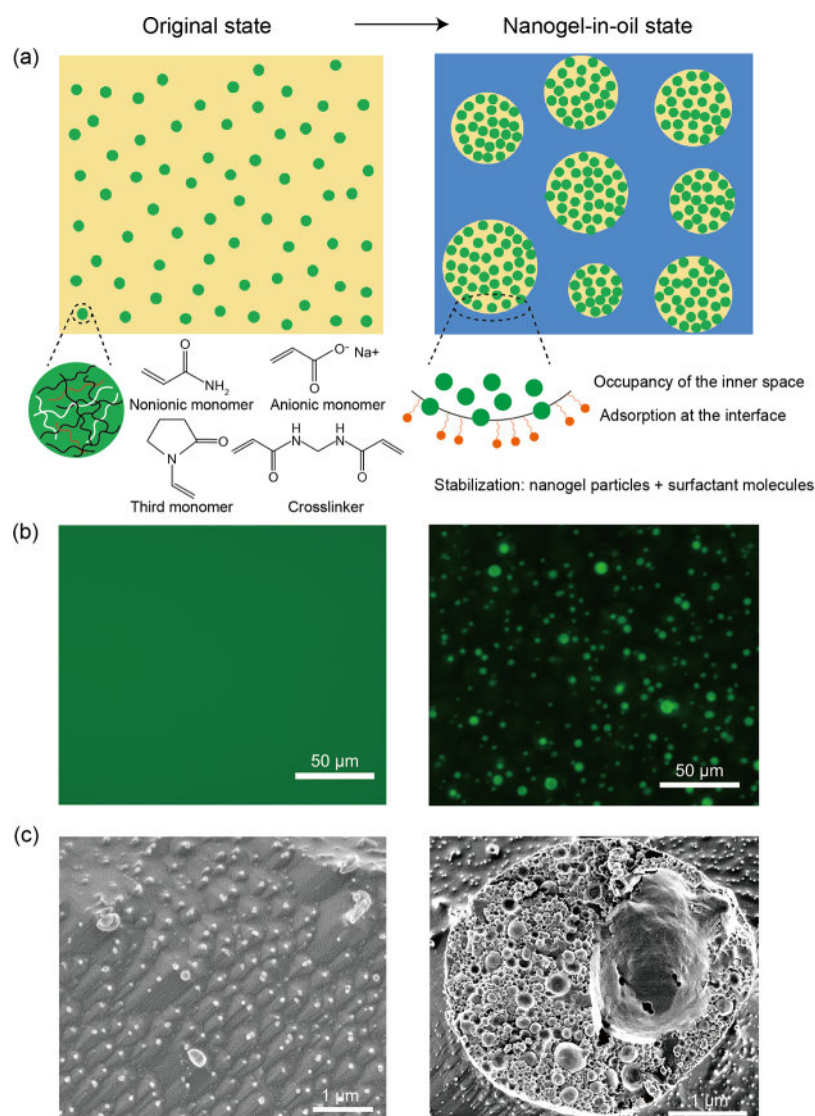


Figure 1. (a) Schematic of the transition from the original state to the nanogel-in-oil state during the synthesis process. The yellow, blue, and green parts represent the oil phase, aqueous phase, and nanogel particles, respectively. The chains inside the nanogel particle with different colors (left) represent the cross-linked network from three different monomers. The orange symbols at the interface (right) denote surfactant molecules as stabilizers. (b) Fluorescence images of the particle distribution in the original stock suspension (left) and the prepared aqueous suspension (right). (c) Cryo-SEM micrographs showing the spotlike nanosized nanogel particles (left) and the inner structure of an oil droplet encapsulating nanogel particles (right).

potential dynamic effects, the pending time was gradually increased until equilibrium, which ranged from approximately 5 to 300 s.

2.4. Static Emulsification Tests. The aqueous suspension and decane were added into glass test tubes with different volume ratios, which were vigorously mixed and stored at ambient temperature until no changes in the phase distribution were observed. For comparison, samples without mixing were also prepared to evaluate the spontaneous emulsification at the interface. The inner structure of the formed emulsions was characterized via an inverted microscope. The viscoelasticity of emulsions was evaluated via oscillation frequency sweep tests using a rheometer (Haake Mars III, Thermo Fisher Scientific, USA) under constant stress conditions, with frequency ranging from 0.1 to 14 Hz.

2.5. Microfluidic Chip Design and Fabrication. The microfluidic chip was constructed based on a multistep reservoir-on-a-chip design paradigm.⁴⁴ The porous medium was regenerated based on microstructure information from real rock samples, which yielded complex geometry, hierarchical characteristics, and wide pore size distribution (Figure S1). The porosity is 44.4%, with 2D pore sizes ranging from 2 to 180 μm .

The microchips were made from silicon wafers, considering the small and dense pore geometries. The fabrication procedure includes image import into AutoCAD, standard photolithography, and inductively coupled plasma-deep reactive ion etching (ICP-DRIE).⁴⁵ The etching depth is equal to the mean pore size (39.5 μm). The patterned wafer was then anodically bonded to a Pyrex glass wafer (Schott). The upstream and downstream ends of the porous structure were drilled with 2 mm diameter holes for the inlet and outlet. The wafers were washed with dilute hydrochloric acid and dichlorodimethylsilane and put in the fume hood for 24 h to keep a stable wettability condition.

2.6. Microfluidic Experimental Setup. The cleaned microchip was fixed by a custom-designed fixture under a stereo-fluorescence microscope (Nikon SMZ18, Japan) after being treated in a vacuum for 12 h. The fluorescent dyed oil (100 ppm of Nile red in decane) was injected as the defending fluid first until the entire pore space was filled. The valve was then switched, and the invading fluid was injected at a constant flow rate. The characteristic capillary number defined as $\text{Ca} = \mu_{\text{inv}}u/\sigma$ was controlled at approximately 1.7×10^{-5} , where μ_{inv} is the viscosity of the invading fluid, u is the average velocity, and σ is the IFT. The waste liquid was collected in the back reservoir under atmospheric

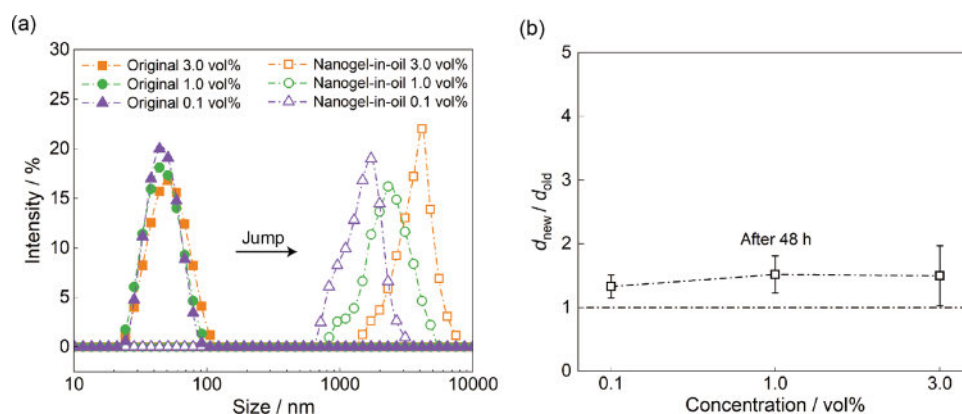


Figure 2. (a) Particle size distribution in the original state and nanogel-in-oil state at different concentrations. (b) Comparison of the average particle size of nanogel-in-oil suspensions immediately after preparation and after standing for 48 h.

pressure. The displacement process lasted until a changeless phase distribution (saturation change less than 1% per 10 PV injections) was reached. Each experiment was repeated three times to ensure the reliability of the displacement performance.

The bandpass wavelengths of the excitation and receiving filters ($\lambda_{\text{ex}} = 460\text{--}500\text{ nm}$ and $\lambda_{\text{em}} = 500\text{--}540\text{ nm}$) were selected to match the excitation and emission wavelengths of the fluorescent nanogel particles and Nile red dissolved in decane. It should be mentioned that the fluorescence intensity of the oil phase was much higher than that of the particles. Hence, the latter posed a negligible impact on the identification and quantification of the phase distribution but can be detected by longtime exposure under a higher resolution.

2.7. Image Processing. Image processing was performed using a self-developed algorithm based on the Image Processing Toolbox of Matlab. For immiscible displacement, the captured image sequences are usually binarized to determine the phase distribution. The invading and defending phases can be readily distinguished with a high signal-to-noise ratio. However, the formation of emulsions makes binarization inapplicable, and the mixed phases at varying degrees are difficult to identify. Therefore, we evaluated the phase distribution based on grayscale analysis. The original RGB images with a time resolution of 1 s were converted to grayscale images and filtered to eliminate noise. The calibration points linking the fluorescence response and oil content were fitted well by a linear relationship (Figure S2). The aqueous phase saturation or displacement efficiency can be calculated as $S = 1 - \frac{\sum_i I_i}{N_0 I_{\text{max}}}$, where I is the local grayscale value, N_0 is the pixel number of the pore space, and I_{max} is the maximal grayscale value representing the pure oil phase. The solid phase was distinguished by a binary image of the oil-saturated state.

We further performed quantitative topological analysis based on the binarization of the grayscale images. Binarization will lead to unavoidable errors in the identification of emulsion phases, where phases with a higher or lower oil content will be recognized as the oil or aqueous phase, respectively. However, topological statistics can provide insightful qualitative information about the displacement enhancement pattern. The Euler number is commonly used to characterize fluid topology, which is defined as $\chi = C_0 - C_1 + C_2$, where C_0 is the number of objects, C_1 is the number of voids, and $C_2 = 0$ for 2D analysis. We counted the total Euler number of the aqueous phase χ_1 to evaluate the path connectivity and phase state. The volume fraction of residual oil clusters A_0 occupying the unswept porous structures ($\chi < 1$) was also calculated.

3. RESULTS AND DISCUSSION

3.1. Colloidal State of Nanogel-in-Oils. Original nanogel particles were synthesized by inverse emulsion polymerization from three kinds of monomers, where acrylamide was the main component. The stock suspension was transparent and uniform, indicating a stable dispersed state. Figure S3 shows the FTIR

spectrum of the cross-linked nanogels. The peaks at 3338 and 3192 cm^{-1} could be assigned to the characteristic stretching vibration of N–H. The stretching vibration absorption peak of C=O can be observed at 1652 cm^{-1} .

As illustrated in Figure 1a, transfer of nanogels from the stock suspension in the oil phase into the aqueous phase produced nanogel-in-oils with a unique colloidal state. By introducing an additional hydrophilic surfactant after polymerization, the phase-state transition from water-in-oil to oil-in-water can be achieved when preparing aqueous suspensions. Following the procedures described in Section 2.1, the nanogel particles will not be released easily via demulsification like microgel particles but remained stable inside the oil droplets and form nanogel-in-oils. On the one hand, the numerous encapsulated nanogels can occupy most of the interior space, limiting the destabilization and collapse of the outer liquid–liquid interface. On the other hand, the extremely small size of nanogel particles contributes to a higher interfacial adsorption tendency, reinforcing the robustness of nanogel-in-oils in conjunction with surfactants released into the bulk aqueous phase.^{46–49}

Figure 1b presents the fluorescence images of the particle distribution in different states. In the stock suspension, a diffuse fluorescence distribution was observed since nanosized particles cannot be identified by optical imaging. Unexpectedly, a large number of micron-sized particles with ideal sphericity appeared in the aqueous suspension. Microscopic morphology captured by cryo-SEM (Figure 1c) verified the formation of nanogel-in-oils, i.e., the micrometer-sized particles were oil droplets encapsulating nanogel particles.

3.2. Suspension Property. The particle size distribution was measured to quantify the colloidal state, as presented in Figure 2a. In the original state, the average particle size was approximately 50 nm, independent of concentration with a narrow size distribution (polydispersity index < 0.1). In the aqueous suspension, the average size jumped to a few microns, which is consistent with the observed nanogel-in-oil state. It was found that the particle size distribution was still unimodal despite increased polydispersity (Table S1), which implies that nanogel-in-oils have become the dominant colloidal state. The average size fell within the range of approximately $2\text{--}4\text{ }\mu\text{m}$. The unimodal feature is significantly different from the microgel-in-oil suspensions reported in the previous work, where particle trapping was forced by adding excess oil, forming unstable aggregates with a low content.³³ For nanogels, spontaneous trapping was the more favorable event, and most particles were

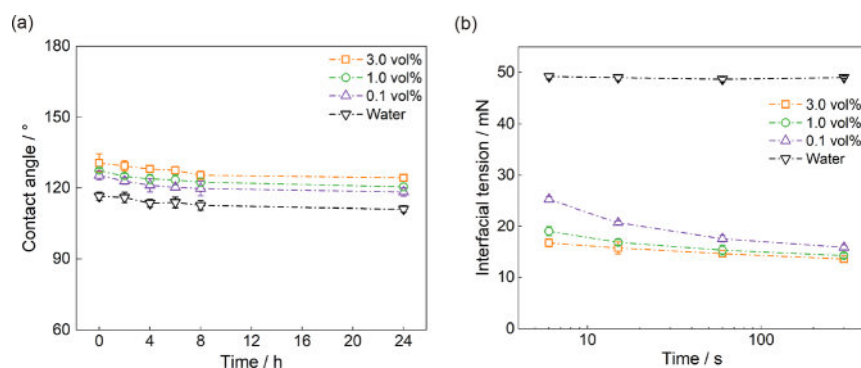


Figure 3. (a) Contact angle changes of aqueous fluid/decane/silicon systems vs time. (b) Interfacial tension changes of aqueous fluid/decane systems vs time.

efficiently encapsulated in micrometer-sized oil droplets. Zeta potential measurements indicated that nanogel-in-oils were negatively charged at all concentrations (Table S1). The electrostatic repulsion between outer droplet surfaces benefits the stabilization of the composite system. The equilibrium state and long-term kinetic stability of nanogel-in-oils were verified by the size variation versus time (Figure 2b). The minor change in average size indicates insignificant coalescence, decomposition, or swelling.

Rheology characterizations show that nanogel-in-oil suspensions exhibit typical shear-thinning behaviors (Figure S4). The samples appeared viscous at 3.0 vol % with an average zero-shear viscosity of approximately 10^3 mPa s. It should be noted that the average shear rate G during displacement experiments was estimated to be approximately 16 s^{-1} using $G = 4U/D$, where U is the average velocity and D is the average pore size. The measured viscosities under such conditions were only slightly larger than pure water, and rheology effects should not be the dominant factor for the phase behaviors and displacement enhancement.

3.3. Interfacial Property. Contact angle and interfacial tension are two important interfacial parameters controlling the multiphase flow. Adsorption of nanogel-in-oils and surfactants onto the interfaces contributed to the variations in the interfacial properties. As shown in Figure 3a, the intrinsic aqueous contact angle increased slightly as the nanogel-in-oil concentration increased, ranging from 110 to 125° . Although the oil-wet state is ordinarily unfavorable for the regular waterflooding process, it was found to promote the development of macroemulsion structures during displacement using nanogel-in-oil suspensions, which will be discussed in Section 3.6. Figure 3b presents the IFT reduction effects, which were stronger than pure particle suspensions but much weaker compared to optimized surfactant solutions.^{40,41}

3.4. Static Emulsifying Behavior in Test Tubes. We investigated the static emulsifying behavior of nanogel-in-oil suspensions for comparison with phase behaviors during displacement. Figure 4a,b indicates that spontaneous emulsification was insignificant, whereas stable emulsions could be produced after vigorous shaking. The formed emulsions were further characterized to identify the phase state. The continuous phase was brighter, attributed to the fluorescence of nanogel particles when using undyed oil, whereas the dispersed droplets were brighter when using dyed oil. Emulsion structures shown in Figure 4c–f demonstrate that the equilibrium state was an oil-in-water macroemulsion, irrespective of the volume ratio, which is in line with the suspension state of nanogel-in-oils. Moreover, a

higher volume ratio of the surrounding aqueous phase led to a reduction in the oil droplet size. The oil-in-water state was also independent of concentration, as shown in Figure 4g. Figure 4h presents the characterization of the viscoelasticity of formed emulsions at 1.0 vol % with equal volumes of the aqueous and oil phases. The storage modulus was always lower than the loss modulus but became close at higher frequencies, which indicates weak viscoelasticity.⁵⁰

3.5. Displacement Performance. A series of displacement experiments was performed on the reservoir-on-a-chip porous structure to visualize the displacement patterns. As shown in Figure 5, the injection of nanogel-in-oil suspensions induced unexpected in situ emulsification in porous media. The invading paths fluctuated and expanded continuously after breakthrough, which provided sufficient contact between the different phases. The discretization of the aqueous phase was more pronounced at higher concentrations and later stages, which induced the emulsion evolution. Differences in color distribution at the final stage indicate differences in the phase state. An increase in the nanogel-in-oil concentration resulted in a larger swept area with enhanced phase mixing.

Figure 6 presents the saturation curves and the corresponding displacement efficiencies. A higher aqueous phase saturation corresponds to a higher displacement performance. The displacement efficiency is defined as $E = (S_0 - S)/S_0$, where S_0 and S are the saturation of the oil phase at the initial and final stages, respectively. The rapid rise at the leftmost part in Figure 6a corresponds to the breakthrough processes, after which the aqueous phase saturation S_a evolved differently. At a low concentration (0.1 vol %), S_a increased continuously but slowly. At an intermediate concentration (1.0 vol %), S_a exhibited a progressively faster rate of increase and achieved the highest displacement efficiency ultimately (71.6%). At a high concentration (3.0 vol %), S_a increased dramatically in the early period, while a reduction appeared at the middle stage and then the curve entered the plateau region. A distinct transition stage with accelerated saturation change was observed at both 1.0 and 3.0 vol %, as denoted in Figure 6a. Significant displacement efficiency enhancements compared to waterflooding were achieved at all concentrations with a nonmonotonic trend versus concentration. Combination of Figures 5 and 6 manifests a close relationship between the development of emulsion phases and enhanced displacement performances.

3.6. Phase Distribution Evolution at the Optimal Concentration. We analyzed and summarized the phase distribution evolution at the optimal concentration based on pore-scale observations to understand the attractive perform-

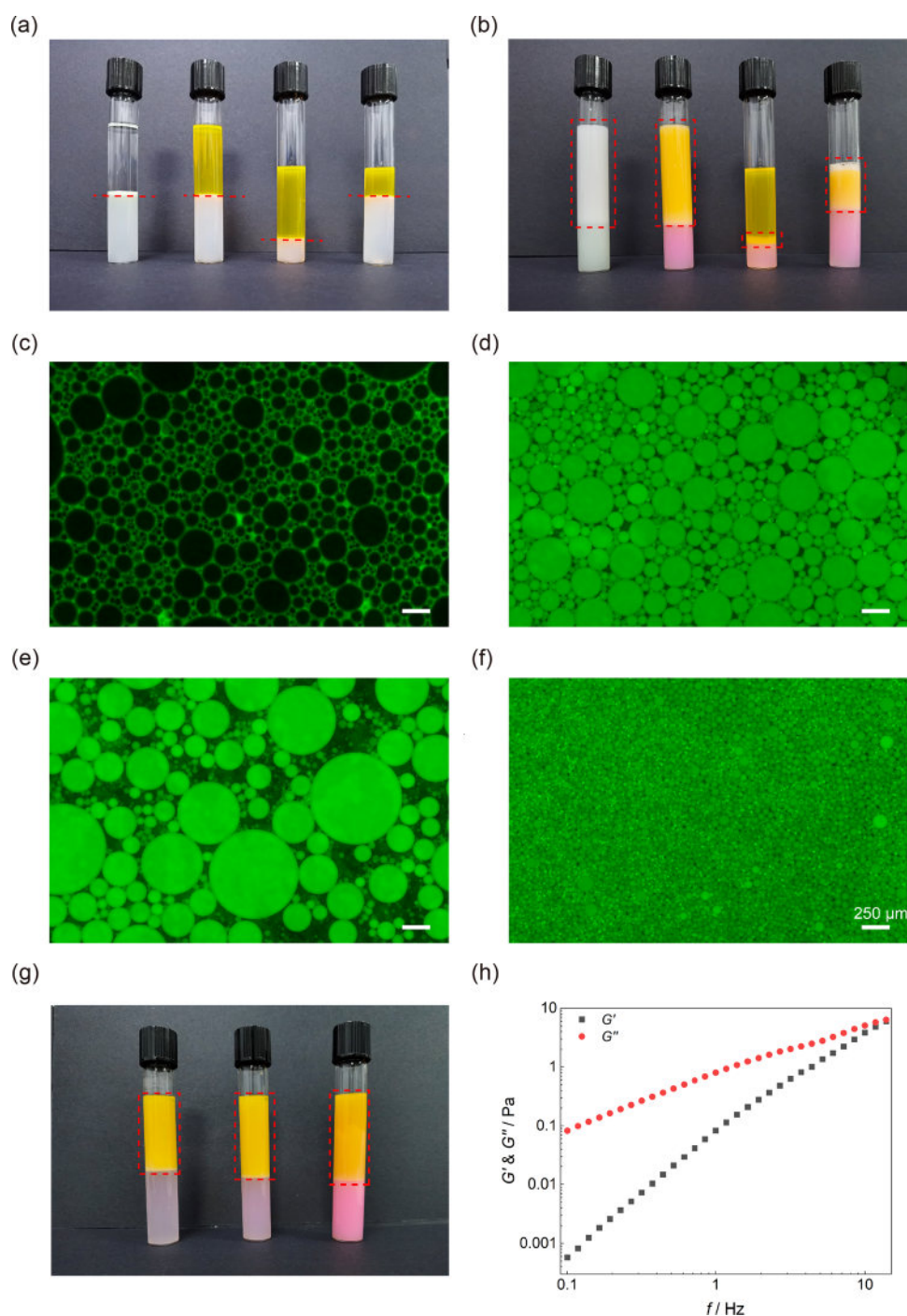


Figure 4. Results of emulsification tests using nanogel-in-oil suspensions. The pictures were taken 1 week after sample preparation. (a,b) Equilibrium phase states in the test tubes at 1.0 vol % nanogel-in-oil concentration without and with mixing, respectively. The dashed lines in (a) denote original phase boundaries, and the dashed boxes in (b) denote emulsified regions. In the leftmost tube, no Nile red was added, and only the fluorescence of nanogel particles in the aqueous phase can be identified. In the other three tubes, Nile red was added, and only the fluorescence of the oil phase with a much higher intensity can be identified. The volume ratios of aqueous and oil phases were 1:1, 1:1, 1:3, and 3:1 from left to right. (c–f) Inner structures of the formed macroemulsions, corresponding to the test tubes from left to right, respectively. (g) Emulsion states at different nanogel-in-oil concentrations (0.1, 1.0, and 3.0 vol %). (h) Typical curves of oscillation frequency sweep tests. The concentration was 1.0 vol %, and the two-phase volume ratio was 1:1.

ance of nanogel-in-oils. At the early stage after breakthrough, emulsion phases have not been fully developed. Aqueous ganglion formation and oil film development were found to be the dominant events during this period.

The breakup of droplets is governed by the interplay between the viscous and interfacial forces, which can be characterized by

the droplet capillary number $Ca_d = \eta_c Gr / \sigma$, where η_c is the viscosity of the continuous phase, G is the stretch or shear rate in extensional or shear flows, respectively, and r is the droplet radius.^{35,51} Droplet breakup occurs above a critical $Ca_{d,c}$, which is ordinarily hard to reach during displacement considering the low-average flow rate, except for ultralow IFT conditions.

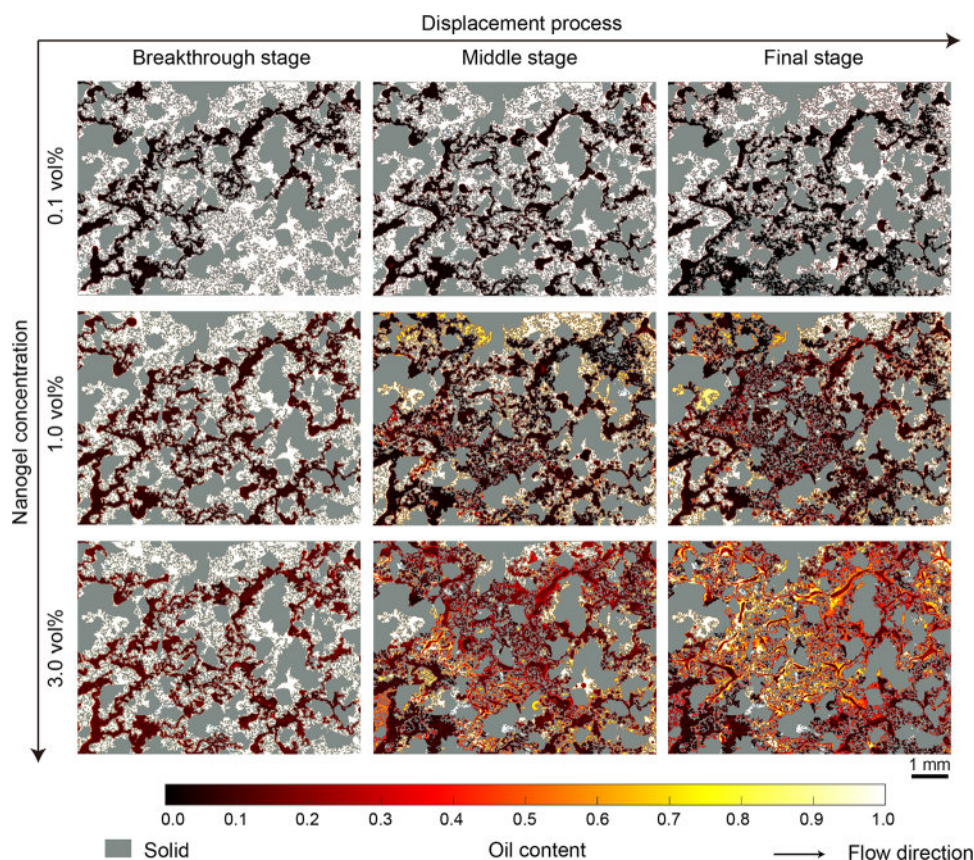


Figure 5. Phase distribution at varying concentrations and displacement stages using nanogel-in-oil suspensions. The middle stage corresponds to half of the time to reach the final stage. The color transition from black or dark red to white corresponds to the local oil content from 0 (pure aqueous phase) to 1 (pure oil phase). The solid part of the porous medium is distinguished from liquid phases and is colored gray.

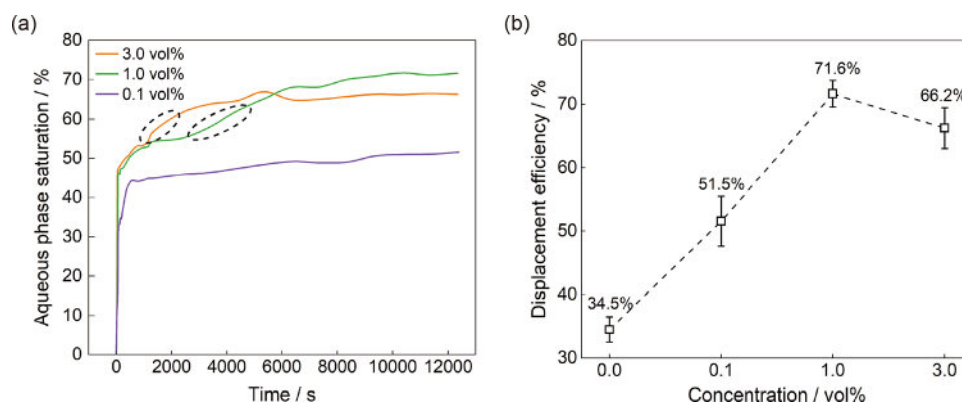


Figure 6. Quantification of the displacement performances. (a) Variations in aqueous phase saturation versus time. The circles denote the transition stages with accelerated saturation changes at 1.0 and 3.0 vol %. (b) Variations in displacement efficiency versus concentration. Result of waterflooding (0.0 vol %) under the same condition is presented for comparison.

However, flow field fluctuations can create instant velocity distribution variations with enhanced stretch and shear actions locally. The irregular geometrical confinement in the disordered structures will further exacerbate the inhomogeneity of the forces exerted on the droplets, promoting breakup events. Figure 7a exemplifies the formation process of an isolated aqueous ganglion. The ganglion was detached from the connected path at the narrow throat after repeated advance and retreat of the displacement front, reflecting the alternation of the flow paths. As shown in Figure 7b, the aqueous phase can be broken at different positions into droplet swarms with varying sizes under persistent flow field fluctuations. The frequent occurrence of

such events discretized the phase distribution and generated a considerable number of aqueous ganglia.

Since the invading network was still continuous without significant phase mixing, the initial flow field fluctuations can only be attributed to the presence of nanogel-in-oils. The micrometer-sized nanogel-in-oils were much smaller than the average pore size, ensuring their propagation throughout the swept regions. Meanwhile, the wide distribution of smaller pores (Figure S1) with a comparable size to nanogel-in-oils greatly increased the probability of particle retention, leading to physical plugging⁸ or capillary resistance.³⁹ Owing to the intermediate property between solid particles and liquid

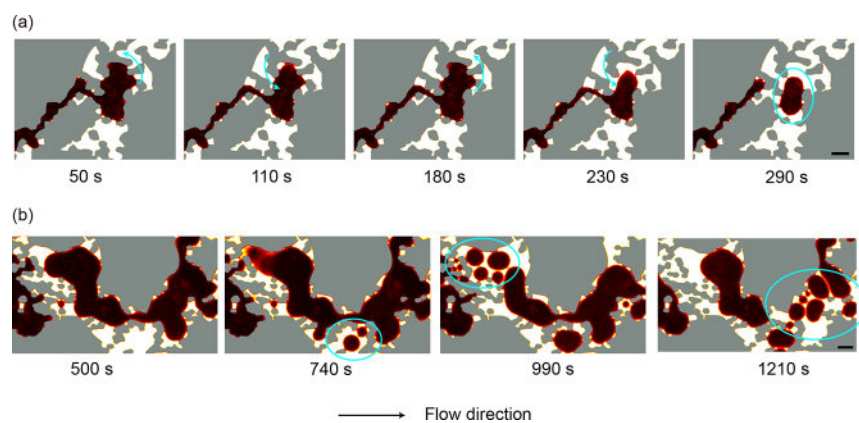


Figure 7. Formation of aqueous ganglia under flow field fluctuations induced by nanogel-in-oils. (a) Detachment of an isolated aqueous ganglion after repeated alternation of the flow direction. (b) Generation, merging, and regeneration of droplet swarms. The scale bars represent 100 μm .

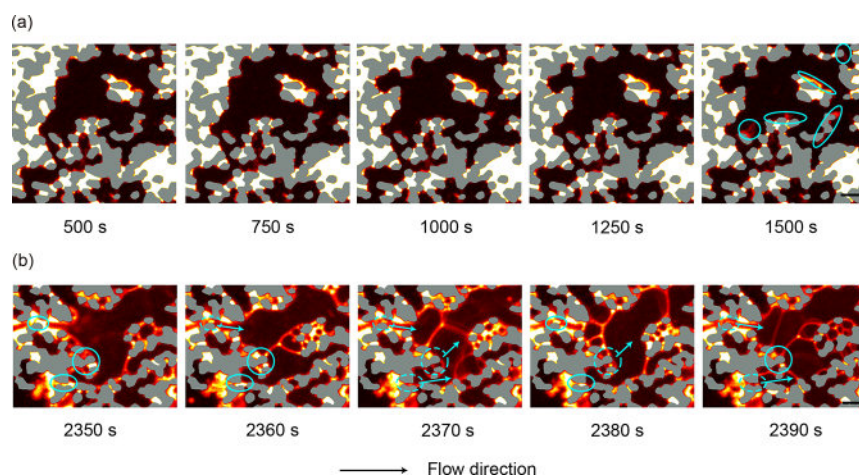


Figure 8. Development of oil films with nanogel-in-oils serving as an additional oil source. (a) Accumulation and thickening of oil films covering solid grains. Typical positions are denoted by circles in the last frame. (b) Formation of foam-like structures. The solid open circles denote the presence of accumulated oil. The dashed circles indicate the reduction in local oil content compared to the previous frame, and the arrows denote their transformation into lamellae attached to the solid grains. The scale bars represent 100 μm .

droplets, nanogel-in-oils can achieve sustainable retention–migration procedures, which facilitate the localized redistribution of pressure and flow rate.

As nanogel-in-oils were essentially oil droplets containing nanogels, they may serve as an additional oil source when transported into the porous medium. Wettability characterizations have shown the oil-wet state of the substrate when using nanogel-in-oil suspensions, which was beneficial for the spreading of the oil films. More importantly, the enhanced affinity of solid grains for nanogel-in-oils promoted their adsorption/deposition onto the solid surface. Figure 8 shows the development of oil films driven by nanogel-in-oils. On the one hand, oil films covering solid grains accumulated and thickened gradually (Figure 8a). The film structures were relatively loose with a lower brightness compared to the bulk phase. On the other hand, the trapped oil at narrow channels was transferred into connected films separating the aqueous phase. As presented in Figure 8b, when the accumulated oil at upstream throats decreased, foam-like structures appeared at downstream pores with lamellae attached to the solid grains. Furthermore, the displaced oil reappeared in the same position, leading to the continuous improvement of emulsion structures. Given that the selected positions were both near the inlet without significant residual oil mobilization during the corresponding period, the

increase in oil content should originate from the invading fluid, i.e., nanogel-in-oils.

The synergistic effects of aqueous phase breakup and oil film development led to the spontaneous formation of water-in-oil macroemulsions throughout the porous medium, as shown in Figure 9. Despite the compact inner structure, their distribution in the porous medium was relatively loose, with a dynamic balance between generation and redistribution. The emulsion phases yielded similar lamella compartment texture to foams,^{52–54} where the tightly packed aqueous droplets occupying most of the volume were separated and stabilized by oil films. Interestingly, the surrounding and dispersed phases were opposite the result of static phase behavior tests, which was governed by the flow conditions. After breakthrough, the flow field fluctuations preferentially induced redistribution of the invading phase, causing aqueous ganglion accumulation. Meanwhile, interconnected oil films supplemented by nanogel-in-oils naturally served as the surrounding phase. In situ development of water-in-oil rather than oil-in-water macroemulsions is more favorable for displacement enhancement since residual oil in discontinuous form should be more difficult to transport.⁵⁵ Considering the components of the aqueous phase, the comprehensive phase state was nanogel-in-oil-in-water-in-oil.

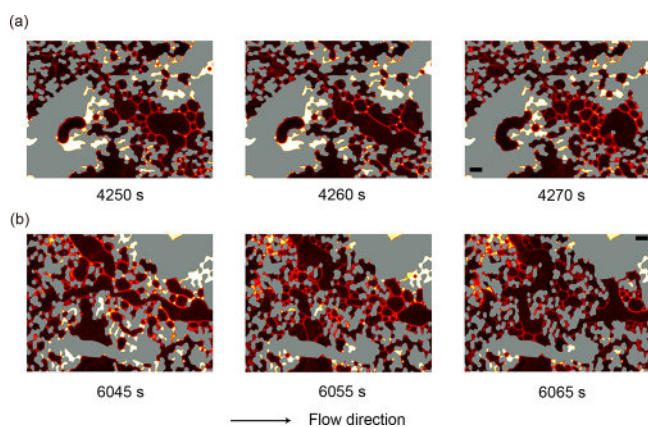


Figure 9. Morphology of water-in-oil macroemulsion phases during rapid evolution. (a, b) Two representative positions with pore size variations benefiting emulsion generation. The scale bars represent 100 μm .

Figure 10 summarizes the typical displacement enhancement modes related to phase distribution evolution. As shown in Figure 10a, the flow resistance that rises in swept regions forced the invasion into unswept regions, which expanded the invading paths and enhanced the sweeping efficiency. Even trapped clusters in dead-end or dead-end-like structures can be displaced and transported in the film state. The occurrence of such events was observed throughout the displacement process. As macroemulsions were gradually developed, residual oil in the nearby regions can be carried away through the thickening of lamellae, which was then transported along the film network (Figure 10b).

3.7. Interpretation of Nonmonotonic Concentration Effect. The nonmonotonic concentration effect originated from the concentration-dependent emulsion evolution. Nanogel-in-oils yielded a significant impact on flow field and phase behaviors, leading to controllable multiphase flow patterns.

The flow field fluctuations were the premise for the development of macroemulsions, where nanogel-in-oils played an important role. The widespread and nonuniform distribution of nanogel-in-oils at the final stage (Figure 11a) suggests complex particle behaviors during displacement processes, as

analyzed in Section 3.6. To investigate the relationship between particle behaviors, flow field fluctuations, and phase distribution changes, we monitored the pressure difference evolution at varying nanogel-in-oil concentrations (Figure 11c). At the early stage after breakthrough, the injection pressures fluctuated at constrained levels. The initial fluctuations induced frequent breakup of droplets and development of emulsion structures, which were strengthened as the nanogel-in-oil concentration increased. Afterward, the pressure difference increased stepwise and reached a higher level at intermediate (1.0 vol %) and high (3.0 vol %) concentrations. The pressure rise was more dramatic at 3.0 vol %, whereas no further development was detected at 0.1 vol %.

The transition in the pressure difference corresponds to the formation of the macroemulsion phases. From the perspective of flow dynamics, the higher surface area contributed to a more effective transfer of shear forces between droplets, resulting in a higher apparent viscosity.² From the perspective of energy balance, the creation of interfaces increased the surface energy, which needs to be provided by additional energy input.⁵⁶ Such transitions, in turn, further enhanced emulsion development. As shown in Figure 11b, the emulsion state at the final stage varied versus nanogel-in-oil concentration, from isolated ganglia at a low concentration to dense emulsions with tiny droplets at a high concentration. As the droplet size decreases, the specific area will increase, which corresponds to an increase in the oil content in water-in-oil macroemulsions. Figure 11d presents the statistics of the oil content distribution based on grayscale analysis. At 1.0 vol %, most emulsion phases exhibited a low oil content with a distinct peak at 10%, indicating compact structures with intermediate droplet diameters. Residual oil can be most effectively mobilized and displaced out in such situations. In contrast, emulsion phases with a middle-to-high oil content (20–80%) occupied a larger volume at 3.0 vol %. Oil trapping in such dense emulsion phases and compression of mainstream paths were responsible for the mobility reduction of residual oil. A higher volume ratio of phases with oil content over 80% observed at 0.1 vol % indicates a relatively stable displacement pattern with larger unswept regions.

Figure 12 presents the evolution of Euler characteristics of the aqueous phase χ_a and volume fraction of oil clusters A_o . Ganglion formation will increase χ_a by increasing the number of

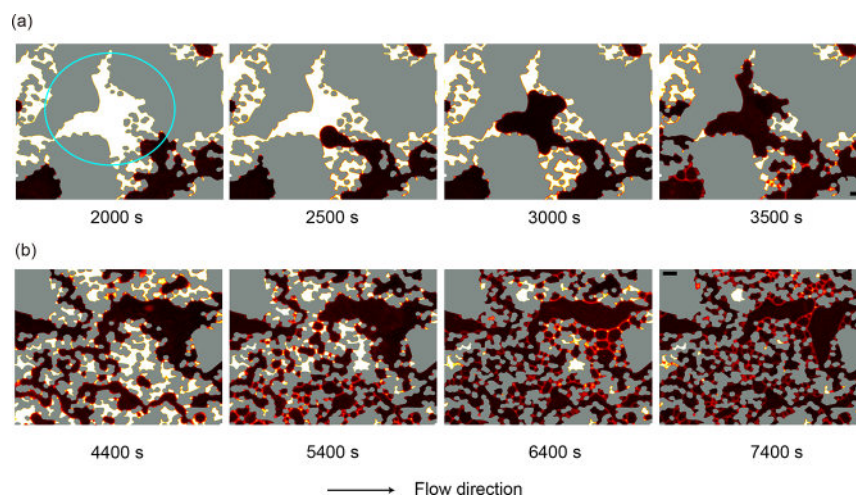


Figure 10. Displacement enhancement modes. (a) Invasion of continuous aqueous phase into unswept regions. (b) Residual oil transport in macroemulsion phases. The scale bars represent 100 μm .

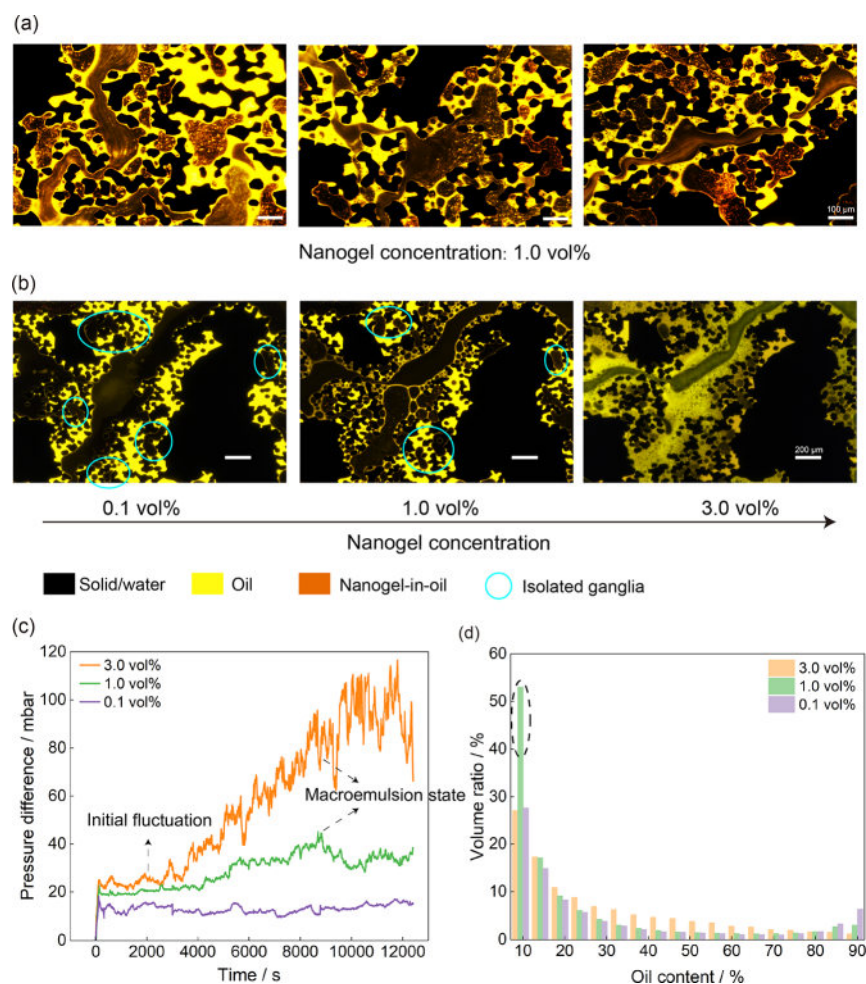


Figure 11. Correspondence between particle behaviors, pressure fluctuations, and emulsion states with variations vs concentration. (a) Particle distribution in the porous medium at 1.0 vol %. The fluorescent nanogel-in-oils appearing orange were identified under longtime exposure and high contrast. (b) Variations in emulsion state vs concentration. The isolated aqueous ganglia are denoted by circles. Local views in (a) and (b) were original fluorescence images captured immediately after displacement experiments. (c) Pressure difference evolution vs time measured at the inlet and outlet. (d) Statistics of oil content distribution at the final stage calculated from grayscale values.

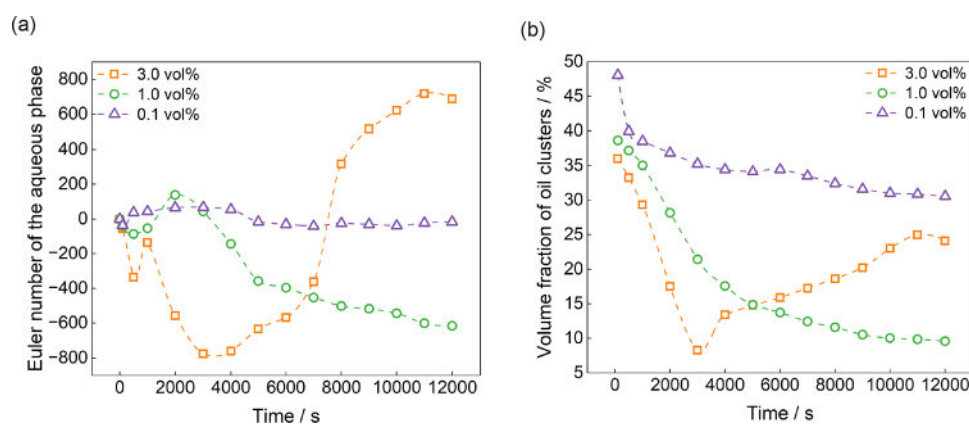


Figure 12. Topological analysis based on binarization. Evolution of (a) Euler characteristic of the aqueous phase and (b) volume fraction of oil clusters after breakthrough. Definition and calculation of the parameters have been introduced in Section 2.7.

isolated elements, whereas invasion in connected paths will decrease χ_a by increasing the number of redundant loops inside the aqueous phase. Both events will lower A_o , as shown in Figure 12b. At a low concentration (0.1 vol %), χ_a fluctuated, while A_o decreased in a limited range. Both aqueous phase breakup and invasion events occur but at a low frequency under weak

fluctuations. At an intermediate concentration (1.0 vol %), χ_a increased rapidly to the peak value after a slight decrease, which is attributed to more frequent ganglion breakup events. The continuous decrease in χ_a afterward governed by invasion events indicates a connected invasion pattern, which corresponds to the formation and development of macroemulsion phases with

optimal features. Throughout the displacement process, A_o decreased continuously and reached the lowest value among all cases in the final stage, which is consistent with the displacement performances. At a high concentration (3.0 vol %), a nonmonotonic evolution of both χ_a and A_o was observed. Before reaching the lowest point, the evolution patterns were similar to that at 1.0 vol % with a shorter accumulation time. The lowest point should correspond to fully developed macroemulsion phases. Considering the emulsion state at the final stage, the anomalous rise afterward was related to the densification of the emulsion and the increase in oil content.

3.8. Comparative Experiments Using Other Dispersed Systems. To elucidate the promising application potential of nanogel-in-oils and clarify the importance of different components, we conducted comparative experiments under similar conditions. Microgel particle suspensions and oil-in-water emulsions excluding nanogels were prepared to investigate the influence of the colloidal state. The characteristic sizes and IFT values were controlled in a close range, as shown in Table 1.

Table 1. Basic Parameters of the Samples for Comparison (1.0 vol %)

type	IFT/mN	average size/nm	displacement efficiency/%
nanogel-in-oil suspension	13.3 ± 0.4	2354.7 ± 329.2	71.6
microgel particle suspension	13.9 ± 0.5	3219.3 ± 219.5	58.1
mineral oil-in-water emulsion	12.5 ± 0.6	2189.2 ± 179.6	37.4
purified nanogel suspension	35.3 ± 0.8	177.5 ± 3.1	43.6

Purified nanogel particle suspensions excluding surfactants and oil were also prepared, which exhibited a much smaller particle size and a larger IFT value. The average size was larger than that of the original state due to adhesion between the polymer chains. Static phase behavior tests indicate that the above suspensions can induce emulsification similar to that of nanogel-in-oil suspensions (Figure S5).

Displacement experiments indicate that all of them yielded weaker performances compared to nanogel-in-oil suspension at the same concentration (Table 1 and Figure S6). At 1.0 vol %, the additional recovery applying nanogel-in-oil suspension compared to waterflooding was approximately 37%, which was over 4 times that of purified nanogel suspension. Despite significant fluctuation of invading paths when using microgel particle suspensions, spontaneous development of macroemulsion phases was not observed. Combining pressure evolution monitoring (Figure S7) and pore-scale observations (Figure S8), it was found that microgel particles caused severe pressure rise of an order of magnitude higher than nanogel-in-oils with harmful clogging, which is adverse to sustained shear action and phase evolution. On the contrary, oil droplets induced much weaker pressure fluctuations with limited retention. Besides, microgel particles cannot supplement additional oil, which also hindered emulsion evolution. Therefore, better mobility and deformability with oil affinity compared to microgel particles and a more stable state with higher mechanical strength compared to oil droplets endowed nanogel-in-oils with the optimal displacement performance. For the purified nanogel suspension, the invading path remained continuous with a changeless phase distribution after break-

through. Plain nanogel particles with a much smaller size posed a minor impact on the invasion pattern. The marginally higher displacement efficiency compared to micrometer-sized oil droplets should be attributed to the hydrophilicity of nanogels. In summary, the joint effects of nanogel particles and oil droplets with the aid of surfactants resulted in attractive properties of composite nanogel-in-oils.

It is worth mentioning that discontinuity of the aqueous phase and formation of water-in-oil macroemulsions have also been reported in some recent studies on surfactant flooding.^{54,57} Nevertheless, the suspensions investigated in this study without cosolvents and additional salt were far away from the optimized surfactant flooding systems, as indicated in IFT measurements and static emulsification tests. The phase-state variations were not confined to the vicinity of interfaces in swept regions but expanded to a broader area with enhanced mixing. Persistent saturation changes at the postbreakthrough stage have been observed at all concentrations.

4. CONCLUSIONS

In this work, we propose a conceptually novel and practically feasible strategy to fabricate composite colloidal systems via encapsulation of polymeric nanogels in oil droplets with a high loading capacity. Nanosized gel particles were transformed into micrometer-sized nanogel-in-oils in aqueous suspensions, which yielded unimodal size distribution and long-term kinetic stability. During displacement in porous media, the in situ development of water-in-oil macroemulsions was observed, which was contrary to the oil-in-water state in static tests. Nanogel-in-oils played a key role in the evolution process. The retention and migration of nanogel-in-oils induced sustainable flow field fluctuations, which promoted the breakup of the aqueous phase. On the other hand, adsorption and accumulation of nanogel-in-oils on oil-wet solid grains served as an additional oil source, which promoted the development of oil films. Both the invasion into unswept regions in continuous paths and residual oil transport through an interconnected lamellar network contributed to the displacement enhancement. Variations in phase distribution evolution versus nanogel-in-oil concentration indicate controllable multiphase flow consequences. A series of comparative experiments show that nanogel-in-oils can achieve the highest displacement efficiency among the tested dispersed systems.

The fabricated nanogel-in-oil suspension system provides a new paradigm for manipulating emulsion evolution via colloidal behaviors that emphasize the importance of flow field adjustment. The intermediate state between solid particles and liquid droplets endows nanogel-in-oils with unique properties for multiphase flow control. The exceptional displacement enhancement effects can be widely utilized in geological systems such as hydrocarbon recovery, soil remediation, and carbon dioxide sequestration. Further efforts are needed for engineering applications of nanogel-in-oils, considering complex environmental conditions. Moving forward, the formation of multiple emulsions induced by nanogel particles reported here may also be extended to the food and cosmetic industry, as well as biomedical research. Self-equilibrium process of nanogel-in-oil formation and the precise control of the suspension property should be carefully evaluated for broader applications. Regardless, our results pose important implications for the utilization of polymer materials and fabrication of composite colloidal systems.

■ ASSOCIATED CONTENT

SI Supporting Information

The Supporting Information is available free of charge at <https://pubs.acs.org/doi/10.1021/acsami.3c05576>.

Microchip design and experimental setup; calibration curve for phase distribution quantification; FTIR spectrum of nanogels; average size and zeta potential of nanogel-in-oils; rheology characterizations of nanogel-in-oil suspensions at different concentrations; emulsification tests using other dispersed systems; phase distribution at the final stage of comparative experiments; and comparison of pressure evolution and pore-scale observations using different injection fluids (PDF)

■ AUTHOR INFORMATION

Corresponding Author

Moran Wang – Department of Engineering Mechanics, Tsinghua University, Beijing 100084, China; orcid.org/0000-0002-0112-5150; Email: mrwang@tsinghua.edu.cn

Author

Xukang Lu – Department of Engineering Mechanics, Tsinghua University, Beijing 100084, China; orcid.org/0000-0003-3315-6389

Complete contact information is available at: <https://pubs.acs.org/doi/10.1021/acsami.3c05576>

Author Contributions

The manuscript was written through contributions of all authors. All authors have given approval to the final version of the manuscript.

Notes

The authors declare no competing financial interest.

■ ACKNOWLEDGMENTS

This work was financially supported by the National Key Research and Development Program of China (No. 2019YFA0708704) and the NSF grant of China (Nos. 12272207 and U1837602). We would like to sincerely acknowledge Dr. Mengquan Shi from the Institute of Physics and Chemistry, Chinese Academy of Sciences, for his help with nanogel synthesis.

■ REFERENCES

- (1) Zhang, H.; Nikolov, A.; Wasan, D. Enhanced Oil Recovery (Eor) Using Nanoparticle Dispersions: Underlying Mechanism and Imbibition Experiments. *Energy Fuels* **2014**, *28* (5), 3002–3009.
- (2) Thomas, S.; Farouq Ali, S. M. Flow of Emulsions in Porous Media, and Potential for Enhanced Oil Recovery. *J. Pet. Sci. Eng.* **1989**, *3* (1), 121–136.
- (3) Jayanti, S.; Britton, L. N.; Dwarakanath, V.; Pope, G. A. Laboratory Evaluation of Custom-Designed Surfactants to Remediate Napl Source Zones. *Environ. Sci. Technol.* **2002**, *36* (24), 5491–5497.
- (4) Pak, T.; Luz, L. F. D. L.; Tosco, T.; Costa, G. S. R.; Rosa, P. R. R.; Archilha, N. L. Pore-Scale Investigation of the Use of Reactive Nanoparticles for in Situ Remediation of Contaminated Groundwater Source. *Proc. Natl. Acad. Sci. U. S. A.* **2020**, *117* (24), 13366–13373.
- (5) Worthen, A. J.; Bagaria, H. G.; Chen, Y.; Bryant, S. L.; Huh, C.; Johnston, K. P. Nanoparticle-Stabilized Carbon Dioxide-in-Water Foams with Fine Texture. *J. Colloid Interface Sci.* **2013**, *391*, 142–151.
- (6) Lawrence, M. J.; Rees, G. D. Microemulsion-Based Media as Novel Drug Delivery Systems. *Adv. Drug Delivery Rev.* **2000**, *45* (1), 89–121.

- (7) Wang, H.; Gao, L.; Fan, T.; Zhang, C.; Zhang, B.; Al-Hartomy, O. A.; Al-Ghamdi, A.; Wageh, S.; Qiu, M.; Zhang, H. Strategic Design of Intelligent-Responsive Nanogel Carriers for Cancer Therapy. *ACS Appl. Mater. Interfaces* **2021**, *13* (46), 54621–54647.
- (8) Bai, B.; Liu, Y.; Coste, J.-P.; Li, L. Preformed Particle Gel for Conformance Control: Transport Mechanism through Porous Media. *SPE Reserv. Eval. Eng.* **2007**, *10* (02), 176–184.
- (9) Destribats, M.; Lapeyre, V.; Wolfs, M.; Sellier, E.; Leal-Calderon, F.; Ravaine, V.; Schmitt, V. Soft Microgels as Pickering Emulsion Stabilisers: Role of Particle Deformability. *Soft Matter* **2011**, *7* (17), 7689–7698.
- (10) Haney, B.; Werner, J. G.; Weitz, D. A.; Ramakrishnan, S. Absorbent-Adsorbates: Large Amphiphilic Janus Microgels as Droplet Stabilizers. *ACS Appl. Mater. Interfaces* **2020**, *12* (29), 33439–33446.
- (11) Louf, J.-F.; Lu, N. B.; O'Connell, M. G.; Cho, H. J.; Datta, S. S. Under Pressure: Hydrogel Swelling in a Granular Medium. *Sci. Adv.* **2021**, *7* (7), No. eabd2711.
- (12) Zhang, H.; Bai, B. Preformed-Particle-Gel Transport through Open Fractures and Its Effect on Water Flow. *SPE J.* **2011**, *16* (02), 388–400.
- (13) Abdulbaki, M.; Huh, C.; Sepehrnoori, K.; Delshad, M.; Varavei, A. A Critical Review on Use of Polymer Microgels for Conformance Control Purposes. *J. Pet. Sci. Eng.* **2014**, *122*, 741–753.
- (14) Ramachandran, V.; Fogler, H. S. Plugging by Hydrodynamic Bridging During Flow of Stable Colloidal Particles within Cylindrical Pores. *J. Fluid Mech.* **1999**, *385*, 129–156.
- (15) Yao, C.; Liu, B.; Li, L.; Zhang, K.; Lei, G.; Steenhuis, T. S. Transport and Retention Behaviors of Deformable Polyacrylamide Microspheres in Convergent–Divergent Microchannels. *Environ. Sci. Technol.* **2020**, *54* (17), 10876–10884.
- (16) Li, Y.; Sariyer, O. S.; Ramachandran, A.; Panyukov, S.; Rubinstein, M.; Kumacheva, E. Universal Behavior of Hydrogels Confined to Narrow Capillaries. *Sci. Rep.* **2015**, *5* (1), 17017.
- (17) Lei, W.; Xie, C.; Wu, T.; Wu, X.; Wang, M. Transport Mechanism of Deformable Micro-Gel Particle through Micropores with Mechanical Properties Characterized by Afn. *Sci. Rep.* **2019**, *9* (1), 1453.
- (18) Yao, C.; Lei, G.; Gao, X.; Li, L. Controllable Preparation, Rheology, and Plugging Property of Micron-Grade Polyacrylamide Microspheres as a Novel Profile Control and Flooding Agent. *J. Appl. Polym. Sci.* **2013**, *130* (2), 1124–1130.
- (19) Dai, C.; Liu, Y.; Zou, C.; You, Q.; Yang, S.; Zhao, M.; Zhao, G.; Wu, Y.; Sun, Y. Investigation on Matching Relationship between Dispersed Particle Gel (Dpg) and Reservoir Pore-Throats for in-Depth Profile Control. *Fuel* **2017**, *207*, 109–120.
- (20) Lin, M.; Zhang, G.; Hua, Z.; Zhao, Q.; Sun, F. Conformation and Plugging Properties of Crosslinked Polymer Microspheres for Profile Control. *Colloids Surf. A: Physicochem. Eng. Asp.* **2015**, *477*, 49–54.
- (21) Zhang, L.; Abbaspourrad, A.; Parsa, S.; Tang, J.; Cassiola, F.; Zhang, M.; Tian, S.; Dai, C.; Xiao, L.; Weitz, D. A. Core–Shell Nanohydrogels with Programmable Swelling for Conformance Control in Porous Media. *ACS Appl. Mater. Interfaces* **2020**, *12* (30), 34217–34225.
- (22) Li, Z.; Zhao, T.; Lv, W.; Ma, B.; Hu, Q.; Ma, X.; Luo, Z.; Zhang, M.; Yu, Z.-Z.; Yang, D. Nanoscale Polyacrylamide Copolymer/Silica Hydrogel Microspheres with High Compressive Strength and Satisfactory Dispersion Stability for Efficient Profile Control and Plugging. *Ind. Eng. Chem. Res.* **2021**, *60* (28), 10193–10202.
- (23) Liu, X.; Zheng, D.; Long, Y.; Wang, L. Highly Robust Nanogels from Thermal-Responsive Nanoparticles with Controlled Swelling for Engineering Deployments. *ACS Appl. Mater. Interfaces* **2023**, *15* (8), 11175–11184.
- (24) Gong, Y.; Zhang, Z.; He, J. Deformation and Stability of Core–Shell Microgels at Oil/Water Interface. *Ind. Eng. Chem. Res.* **2017**, *56* (50), 14793–14798.
- (25) Gong, Y.; Wang, M.; Zhang, Z.; He, J. Microgel Evolution at Three-Phase Contact Region and Associated Wettability Alteration. *Colloids Surf. A: Physicochem. Eng. Asp.* **2018**, *558*, 297–302.
- (26) Zhang, Y.; Geng, J.; Liu, J.; Bai, B.; He, X.; Wei, M.; Deng, W. Direct Pore-Level Visualization and Verification of in Situ Oil-in-Water

Pickering Emulsification During Polymeric Nanogel Flooding for EOR in a Transparent Three-Dimensional Micromodel. *Langmuir* **2021**, *37* (45), 13353–13364.

(27) Torres, O.; Andablo-Reyes, E.; Murray, B. S.; Sarkar, A. Emulsion Microgel Particles as High-Performance Bio-Lubricants. *ACS Appl. Mater. Interfaces* **2018**, *10* (32), 26893–26905.

(28) Torres, O.; Murray, B.; Sarkar, A. Emulsion Microgel Particles: Novel Encapsulation Strategy for Lipophilic Molecules. *Trends Food Sci. Technol.* **2016**, *55*, 98–108.

(29) An, E.; Jeong, C. B.; Cha, C.; Kim, D. H.; Lee, H.; Kong, H.; Kim, J.; Kim, J. W. Fabrication of Microgel-in-Liposome Particles with Improved Water Retention. *Langmuir* **2012**, *28* (9), 4095–4101.

(30) Pautot, S.; Frisken, B. J.; Weitz, D. A. Engineering Asymmetric Vesicles. *Proc. Natl. Acad. Sci. U. S. A.* **2003**, *100* (19), 10718–10721.

(31) Candau, F.; Leong, Y. S.; Pouyet, G.; Candau, S. Inverse Microemulsion Polymerization of Acrylamide: Characterization of the Water-in-Oil Microemulsions and the Final Microlatexes. *J. Colloid Interface Sci.* **1984**, *101* (1), 167–183.

(32) Liu, J.; Almakimi, A.; Wei, M.; Bai, B.; Ali Hussein, I. A Comprehensive Review of Experimental Evaluation Methods and Results of Polymer Micro/Nanogels for Enhanced Oil Recovery and Reduced Water Production. *Fuel* **2022**, *324*, No. 124664.

(33) Lei, W.; Lu, X.; Wu, T.; Yang, H.; Wang, M. High-Performance Displacement by Microgel-in-Oil Suspension in Heterogeneous Porous Media: Microscale Visualization and Quantification. *J. Colloid Interface Sci.* **2022**, *627*, 848–861.

(34) Winsor, P. A. Hydrotrophy, Solubilisation and Related Emulsification Processes. *Trans. Faraday Soc.* **1948**, *44*, 376–398.

(35) Walstra, P. Principles of Emulsion Formation. *Chem. Eng. Sci.* **1993**, *48* (2), 333–349.

(36) Xu, K.; Zhu, P.; Colon, T.; Huh, C.; Balhoff, M. A Microfluidic Investigation of the Synergistic Effect of Nanoparticles and Surfactants in Macro-Emulsion-Based Enhanced Oil Recovery. *SPE J.* **2017**, *22* (02), 459–469.

(37) Romero, M. I.; Carvalho, M. S.; Alvarado, V. Experiments and Network Model of Flow of Oil-Water Emulsion in Porous Media. *Phys. Rev. E* **2011**, *84* (4), No. 046305.

(38) Liu, Z.; Li, Y.; Luan, H.; Gao, W.; Guo, Y.; Chen, Y. Pore Scale and Macroscopic Visual Displacement of Oil-in-Water Emulsions for Enhanced Oil Recovery. *Chem. Eng. Sci.* **2019**, *197*, 404–414.

(39) Ding, B.; Shi, L.; Dong, M. Conformance Control in Heterogeneous Two-Dimensional Sandpacks by Injection of Oil-in-Water Emulsion: Theory and Experiments. *Fuel* **2020**, *273*, No. 117751.

(40) Tagavifar, M.; Xu, K.; Jang, S. H.; Balhoff, M. T.; Pope, G. A. Spontaneous and Flow-Driven Interfacial Phase Change: Dynamics of Microemulsion Formation at the Pore Scale. *Langmuir* **2017**, *33* (45), 13077–13086.

(41) Alzahid, Y. A.; Mostaghimi, P.; Walsh, S. D. C.; Armstrong, R. T. Flow Regimes During Surfactant Flooding: The Influence of Phase Behaviour. *Fuel* **2019**, *236*, 851–860.

(42) Borji, M.; Kharrat, A.; Ott, H. Comparability of in Situ Crude Oil Emulsification in Phase Equilibrium and under Porous-Media-Flow Conditions. *J. Colloid Interface Sci.* **2022**, *615*, 196–205.

(43) Lei, W.; Li, Q.; Yang, H.-E.; Wu, T.-J.; Wei, J.; Wang, M. Preferential Flow Control in Heterogeneous Porous Media by Concentration-Manipulated Rheology of Microgel Particle Suspension. *J. Pet. Sci. Eng.* **2022**, *212*, No. 110275.

(44) Lei, W.; Liu, T.; Xie, C.; Yang, H.; Wu, T.; Wang, M. Enhanced Oil Recovery Mechanism and Recovery Performance of Micro-Gel Particle Suspensions by Microfluidic Experiments. *Energy Sci. Eng.* **2020**, *8* (4), 986–998.

(45) Chomsurin, C.; Werth, C. J. Analysis of Pore-Scale Nonaqueous Phase Liquid Dissolution in Etched Silicon Pore Networks. *Water Resour. Res.* **2003**, *39* (9), 1643.

(46) Dinsmore, A. D.; Hsu, M. F.; Nikolaidis, M. G.; Marquez, M.; Bausch, A. R.; Weitz, D. A. Colloidosomes: Selectively Permeable Capsules Composed of Colloidal Particles. *Science* **2002**, *298* (5595), 1006–1009.

(47) He, Y.; Wu, F.; Sun, X.; Li, R.; Guo, Y.; Li, C.; Zhang, L.; Xing, F.; Wang, W.; Gao, J. Factors That Affect Pickering Emulsions Stabilized by Graphene Oxide. *ACS Appl. Mater. Interfaces* **2013**, *5* (11), 4843–4855.

(48) Baret, J.-C.; Kleinschmidt, F.; El Harrak, A.; Griffiths, A. D. Kinetic Aspects of Emulsion Stabilization by Surfactants: A Microfluidic Analysis. *Langmuir* **2009**, *25* (11), 6088–6093.

(49) Ding, S.; Serra, C. A.; Vandamme, T. F.; Yu, W.; Anton, N. Double Emulsions Prepared by Two-Step Emulsification: History State-of-the-Art and Perspective. *J. Control. Release* **2019**, *295*, 31–49.

(50) Barnes, H. A. Rheology of Emulsions — a Review. *Colloids Surf. A: Physicochem. Eng. Asp.* **1994**, *91*, 89–95.

(51) Bentley, B. J.; Leal, L. G. An Experimental Investigation of Drop Deformation and Breakup in Steady Two-Dimensional Linear Flows. *J. Fluid Mech.* **1986**, *167*, 241–283.

(52) Lemlich, R. Adsorptive Bubble Separation Methods—Foam Fractionation and Allied Techniques. *Ind. Eng. Chem.* **1968**, *60* (10), 16–29.

(53) Almajid, M. M.; Kovscek, A. R. Pore-Level Mechanics of Foam Generation and Coalescence in the Presence of Oil. *Adv. Colloid Interface Sci.* **2016**, *233*, 65–82.

(54) Kharrat, A.; Brandstätter, B.; Borji, M.; Ritter, R.; Arnold, P.; Fritz-Popovski, G.; Paris, O.; Ott, H. Development of Foam-Like Emulsion Phases in Porous Media Flow. *J. Colloid Interface Sci.* **2022**, *608*, 1064–1073.

(55) Kovscek, A. R.; Wong, H.; Radke, C. J. A Pore-Level Scenario for the Development of Mixed Wettability in Oil Reservoirs. *AIChE J.* **1993**, *39* (6), 1072–1085.

(56) Reynolds, C. A.; Menke, H.; Andrew, M.; Blunt, M. J.; Krevor, S. Dynamic Fluid Connectivity During Steady-State Multiphase Flow in a Sandstone. *Proc. Natl. Acad. Sci. U. S. A.* **2017**, *114* (31), 8187–8192.

(57) Yang, W.; Fu, C.; Du, Y.; Xu, K.; Balhoff, M. T.; Weston, J.; Lu, J. Dynamic Contact Angle Reformulates Pore-Scale Fluid-Fluid Displacement at Ultralow Interfacial Tension. *SPE J.* **2021**, *26* (03), 1278–1289.